ACS APPLIED MATERIALS & INTERFACES

Letter

www.acsami.org

Elements Provide a Clue: Nanoscale Characterization of Thin-Film Composite Polyamide Membranes

Xinglin Lu,[†,‡] Siamak Nejati,[†,§] Youngwoo Choo,[§] Chinedum O. Osuji,[§] Jun Ma,[*,‡] and Menachem Elimelech[*,§]

[‡]State Key Laboratory of Urban Water Resource and Environment, Harbin Institute of Technology, Harbin 150090, China

[§]Department of Chemical and Environmental Engineering, Yale University, New Haven, Connecticut 06520-8286, United States

Supporting Information

ABSTRACT: In this study, we exploit the nitrogen−sulfur elemental contrast of thin-film composite (TFC) polyamide membranes and present, for the first time, the application of two elemental analysis techniques, scanning transmission electron microscopy−energy-dispersive X-ray spectroscopy (STEM−EDX) and X-ray photoelectron spectroscopy (XPS) C_{60}^+ ion-beam sputtering, to elucidate the nanoscale structure and chemical composition of the polyamide−polysulfone interface. Although STEM−EDX elemental mapping depicts the presence of a dense polyamide layer at the interface, it is incapable of resolving the elemental contrast at nanoscale resolution at the interfacial zone. Depth-resolved XPS C_{60}^+ ion-beam sputtering enabled nanoscale characterization of the polyamide−polysulfone interface and revealed the presence of a heterogeneous layer that contains both polyamide and polysulfone signatures. Our results have important implications for future studies to elucidate the structure−property−performance relationship of TFC membranes.

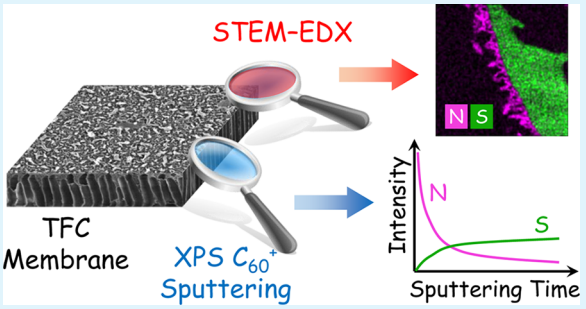

KEYWORDS: *thin-film composite membrane, polyamide−polysulfone interface, elemental contrast, nanoscale characterization*

Reverse osmosis desalination is a vital membrane technology to produce freshwater from saline water sources to address the global challenge of water scarcity.[1,2] Thin-film composite (TFC) membranes are the state-of-the-art for membrane desalination because of their high water permeability and salt selectivity, and their wide pH operation range.[2−4] In addition, the ability to separately optimize two layers, a dense active (selective) layer and a porous support layer, during membrane fabrication renders TFC membranes superior compared to asymmetric membranes formed by phase inversion.[3]

The ultrathin (<500 nm) active layer of TFC membranes is fabricated on top of a porous support layer through interfacial polymerization.[2−4] Surface characteristics (e.g., morphology, functional groups, charge, and hydrophilicity) of the active layer play a significant role in determining TFC membrane performance, including transport properties and fouling propensity.[5−10] Thus, numerous efforts[11−17] have been dedicated to surface characterization of the active layer in order to understand more deeply the relationship between surface properties and TFC membrane performance for guiding membrane design.

During interfacial polymerization, the support membrane, prewetted with aqueous amine solution, is exposed to acyl chloride dissolved in an organic solvent. Monomers diffuse toward the interface between the aqueous solution and organic solvent, where a polycondensation reaction takes place to form the thin active layer.[3,4] Previous studies attributed differences in active layer characteristics to the different interfacial polymerization conditions.[3,7,18,19] Recent studies[20−24] have gradually led to the realization that the active layer characteristics are also significantly influenced by the surface properties of the support layer. In particular, these studies have suggested that the support layer−polyamide interface, particularly pore size and hydrophilicity of the polysulfone support, can impact water permeability and salt rejection of the membrane as well as the morphology of the polyamide active layer. These findings imply that the active layer−support layer interface, where the polyamide thin film adheres to the polysulfone surface, is important for TFC membrane performance.

Efforts to elucidate the structure and composition of the interfacial region have not yet resulted in an analytical toolset that provides both the spatial resolution and chemical sensitivity required to gain insights on the active layer−support layer interface. In regular bright-field or dark-field images taken by scanning electron microscopy (SEM) and transmission electron microscopy (TEM), only limited structural and characteristic information could be gained due to substantial difficulty in discerning interfacial domains.[24−27] Isolation of the polyamide active layer by dissolving the underlying polysulfone support with an organic solvent indirectly provided information

Received: June 19, 2015
Accepted: July 27, 2015
Published: July 27, 2015

DOI: 10.1021/acsami.5b05478
ACS Appl. Mater. Interfaces 2015, 7, 16917−16922

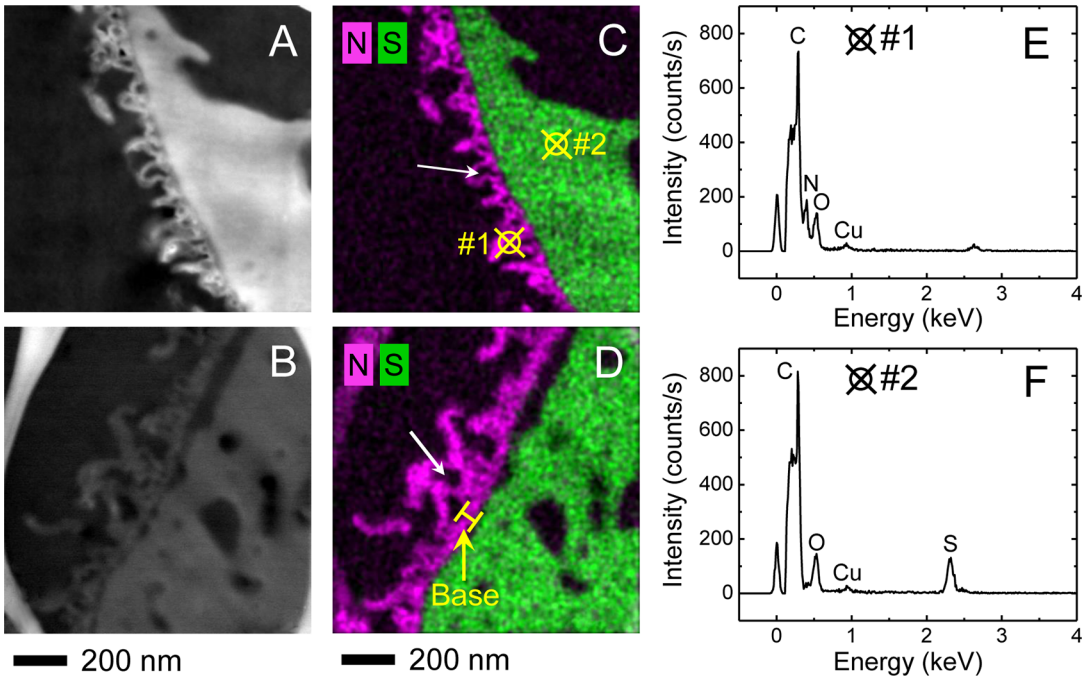

Figure 1. Dark-field TEM cross-section images of (A) NMP-TFC and (B) DMF-TFC membranes. STEM−EDX elemental mappings of (C) NMP-TFC and (D) DMF-TFC membranes, where "N" (magenta) denotes nitrogen and "S" (green) denotes sulfur; the white arrows indicate the cavities inside the ridge structure, while the yellow arrow and bracket indicate the dense polyamide layer. EDX spectra of (E) #1 point and (F) #2 point of the NMP-TFC membrane (shown in C). The thickness of the thin cross-section of the membranes is ∼60 nm. Scale bars are 200 nm.

about structural characteristics of the interface through studying the morphology of the active layer back surface.[27,28] However, because organic solvents can also dissolve some fraction of the polyamide,[26,29,30] the interfacial structure of the isolated polyamide film might not represent the actual interfacial structure of an integral TFC membrane. Therefore, developing a direct characterization method to study the active−support interfacial structure is of paramount importance to provide a more comprehensive understanding of interfacial polymerization and guide support layer design for high-performance TFC membranes.

In this study, we demonstrate, for the first time, the application of two elemental analysis techniques, scanning transmission electron microscopy−energy-dispersive X-ray spectroscopy (STEM−EDX) and X-ray photoelectron spectroscopy (XPS) C_{60}^{+} ion-beam sputtering, for nanoscale characterization of the polyamide−polysulfone interface of TFC membranes. STEM−EDX resolved the membrane structure at mesoscale (<100 nm) resolution and confirmed the presence of a dense layer underneath the nodular structure of the polyamide. XPS depth profiling with nanoscale (<10 nm) resolution revealed the existence of a heterogeneous layer at the interface, where both polysulfone and polyamide signals can be detected concomitantly. Our results highlight the potential implications of these characterization techniques for better understanding of the structure−property−performance relationship of TFC membranes.

To fabricate support layers with different pore size and morphology, we prepared polymer dope solutions using 12 wt % polysulfone in *N*-methyl-2-pyrrolidone (NMP) or dimethylformamide (DMF). An identical interfacial polymerization process was performed on the polysulfone supports to form the polyamide active layer. We denote the TFC membranes cast with NMP and DMF solvents as NMP-TFC and DMF-TFC, respectively. Details on the TFC membrane fabrication are provided in the Supporting Information.

The transport properties of the fabricated TFC membranes are tabulated in Table S1. The water permeability coefficient, *A*, of the DMF-TFC membrane (3.14 ± 0.02 L m^{-2} h^{-1} bar^{-1}) was significantly higher than that of the NMP-TFC membrane (1.73 ± 0.33 L m^{-2} h^{-1} bar^{-1}), whereas the salt permeability, *B*, of the DMF TFC membrane (0.60 ± 0.31 L m^{-2} h^{-1}) was comparable to that of the NMP-TFC membrane (0.50 ± 0.11 L m^{-2} h^{-1}).

SEM micrographs showed that the DMF-polysulfone support layer (Figure S1B) has larger pores on the surface compared to the NMP-polysulfone support (Figure S1A). These results suggest that larger surface pores on the support layer result in a more permeable TFC membrane.[24] After interfacial polymerization, small nodular protrusions dominated the polyamide surface of the NMP-TFC membrane (Figure S1C), compared to the larger leaf-like structure on the DMF-TFC membrane surface (Figure S1D). This difference in surface morphology resulted in higher surface roughness for the DMF-TFC membrane relative to the NMP-TFC membrane,[22] as indicated by the roughness parameters (i.e., R_{rms}, R_a, and R_{max}) in Table S1.

Because the TFC membranes were fabricated through an identical process, except for the solvents (NMP or DMF) used in casting the polysulfone support, we propose that the differences in transport properties and surface morphology of the TFC membranes are attributable to the different surface structures of the underlying polysulfone support layers. Hence, it is imperative to further characterize the chemical composition and structure of the polyamide−polysulfone interface.

Figures 1A, B depict regular TEM cross-sectional images of the TFC membranes. A ridge-and-valley structure, typical of TFC polyamide membranes,[2,3] was observed on both

DOI: 10.1021/acsami.5b05478
ACS Appl. Mater. Interfaces 2015, 7, 16917−16922

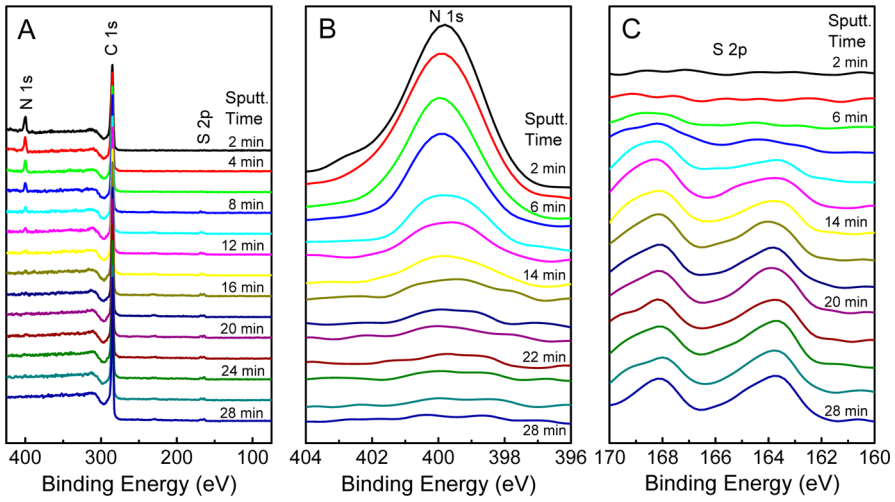

Figure 2. XPS C_{60}^+ ion-beam sputtering depth profiles of the NMP-TFC membrane: (A) survey spectra of 0−450 eV, (B) high-resolution spectra of nitrogen (N 1s orbital), and (C) high-resolution spectra of sulfur (S 2p orbital). The sputtering time was set to 2 min and the spectra were acquired with 30 s wait time after each sputtering. Both survey and high-resolution spectra were acquired over a spot on the membrane surface of approximately 200 μm in diameter with ~50 W beam power. For depth profiling, a C_{60}^+ ion beam with 10 nA beam current were used in the Compucentric Zalar mode to raster over an area of 8 mm in diameter on the membrane surface. For the survey spectra, pass energy is of 117 eV over the range of 0−450 eV with 1 eV resolution and 100 ms dwell time, and averaged over four scans. High-resolution XPS spectra of S 2p and N 1s were acquired with 0.1 eV resolution and 97 eV pass energy with 200 ms dwell time, and averaged over 10 scans. The spectra were shifted using C 1s at 284.8 eV as the internal reference to correct for charging.

membrane surfaces. However, since the polyamide and the polysulfone layers exhibited comparable brightness, it was difficult to accurately discern the polyamide−polysulfone interface, as was also indicated by a previous study.[27] Additionally, because of variations in sample preparation (e.g., thickness of the section) and TEM imaging condition (e.g., contrast and brightness settings), the TEM images showed different levels of contrast. We also note that the image of the NMP-TFC membrane (Figure 1A) was brighter than that of the DMF-TFC membrane (Figure 1B), which further limited direct comparison of the interfacial structure of the two TFC membranes.

Because the polyamide active layer is rich in nitrogen while the underlying polysulfone support layer contains sulfur but no nitrogen, this elemental contrast allows us to perform STEM−EDX measurements to investigate the polyamide−polysulfone interface of TFC membranes. The STEM−EDX elemental mappings are depicted in Figures 1C, D. We present the EDX spectra of two representative points (i.e., points #1 and #2 in Figure 1C) in Figures 1E, F. The EDX spectra of point #1 (Figure 1E), which was located in the polyamide layer, showed a clear nitrogen peak, while that of point #2 (Figure 1F), representing the polysulfone layer, exhibited a clear sulfur peak. Through mapping of these elements on the STEM images, we observed clear cross-section structures for both membranes. Generally, the NMP-TFC membrane (Figure 1C) contained small nodular protrusions on the surface, while the DMF-TFC membrane (Figure 1D) showed a surface with larger leaf-like ridges. These results are consistent with what we observed in the SEM micrographs (Figure S1C, D). The different surface morphology resulted in a thicker polyamide layer for the DMF-TFC membrane (171 ± 10 vs 132 ± 28 nm for the NMP-TFC, Table S1) and higher surface roughness, as indicated above. Additionally, STEM−EDX images clearly indicate the presence of cavities inside the ridge structure of both membranes (as indicated by the white arrows in Figures 1C, D), suggesting the polyamide film is not a homogeneous film throughout its depth.[31,32]

Taking advantage of the nitrogen−sulfur elemental contrast, the polyamide−polysulfone interface was more easily discerned in the STEM−EDX images. At the polyamide−polysulfone interface, the DMF-TFC membrane comprised a continuous 40−70 nm polyamide base (indicated by the yellow arrow and bracket in Figure 1D), from which the ridge-and-valley structure extended outward. This polyamide base structure was also observed on commercial polyamide TFC membranes.[27] On the other hand, the NMP-TFC membrane did not have such a polyamide base and the nodules were directly rooted on the polysulfone surface. We attribute the differences in the polyamide layer structures to the different surface pore structure of the underlying polysulfone support layers. As shown in the Supporting Information, the DMF-polysulfone support has larger surface pores (Figure S1) and higher surface porosity (Table S1), which could contain more *m*-phenylenediamine (MPD) solution during membrane fabrication. When the support membrane is brought into contact with trimesoyl chloride (TMC) during interfacial polymerization, more MPD would diffuse outward to form the continuous polyamide base at the interface.

To further understand the interfacial characteristics of the TFC membranes, XPS C_{60}^+ ion-beam sputtering was performed on the active layer of the membranes. By exploiting the high sensitivity of XPS, we expected to have a more direct exploration of the polysulfone−polyamide interface at the atomic level. Details on the XPS C_{60}^+ ion-beam sputtering experiments are provided in the Supporting Information.

Figure 2A presents a summary of the XPS survey spectra as a function of sputtering time for the NMP-TFC membrane. Generally, we observed a decrease in the intensity of N 1s with an increase of sputtering time from the top (2 min) to the bottom (28 min), while the sulfur peak showed a gradual increase. The trends are more clearly depicted in the high-resolution N 1s spectra (Figure 2B) and S 2p spectra (Figure 2-

DOI: 10.1021/acsami.5b05478
ACS Appl. Mater. Interfaces 2015, 7, 16917−16922

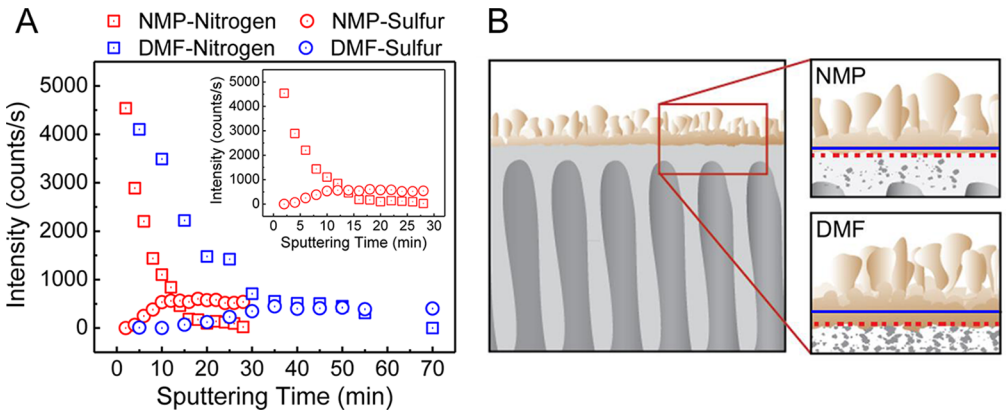

Figure 3. (A) XPS depth profile of the TFC membranes. The intensity for each point was estimated from the integration of the peak areas in high-resolution spectra. (B) Schematics of the interface of the two types of TFC membranes illustrating the difference in the support dense layer structure close to the top surface. The blue solid lines indicate the upper boundary of the polysulfone support layer and the red dashed lines indicate the lower boundary of the polyamide active layer. The gap between the blue and red lines illustrates the heterogeneous layer.

C). The results clearly show that the N 1s peak gradually decreased and finally disappeared at ~20 min, indicating that the ion beam had already reached the pure polysulfone layer. An opposite trend is observed for the S 2p peak, which began to appear at 6 min sputtering time and remained unchanged after 14 min. As shown in Figure S2, the DMF-TFC membrane exhibited trends similar to the NMP-TFC membrane in both nitrogen and sulfur peaks. We also note that the S 2p spectra show two peaks at 168 and 163.5 eV (Figure S2D). The 168 eV peak is attributed to the presence of sulfone groups (O═S═O) on the polysulfone structure.[33] We surmise that the peak at 163.5 eV is ascribed to the presence of sulfide groups,[34] resulting from sulfone group reduction due to exposure of polysulfone to the C_{60}^+ ion beam.

We integrated the peak area in the high-resolution spectra and plotted the data versus sputtering time in Figure 3. The decay of the nitrogen signal and the growth of the sulfur signal are more rapid for the NMP-TFC membrane than the DMF-TFC membrane. We infer from these observations that it takes less time for the C_{60}^+ ion beam to sputter through the NMP membrane, with its sparse ridge-and-valley polyamide structure, compared to the DMF-TFC membrane with the additional polyamide base (Figure 1D), as discussed earlier.

Notably, we reveal a heterogeneous layer containing both polyamide and polysulfone signatures on both TFC membranes. For the NMP-TFC membrane (inset of Figure 3A), the sulfur signal reached a plateau at 14 min and remained constant after that, while the nitrogen signal showed a gradual decrease until 28 min. These results indicate that the ion beam already reached domains mostly occupied by polysulfone with minor detectable polyamide, thus suggesting a heterogeneous layer with ~14 min sputtering time gap. On the other hand, the DMF-TFC membrane exhibited a heterogeneous layer of 30 min sputtering time gap. These results suggest that the DMF-TFC membrane has a much thicker heterogeneous layer compared to that of NMP-TFC membrane, as illustrated in Figure 3B. We surmise this variation is attributable to the different surface pore structure of the polysulfone supports. The DMF-polysulfone support (Figure S1B) has larger surface pores, which lead to formation of polyamide deeper in the polysulfone compared to the NMP-TFC membrane.[24,35]

We have shown that the XPS depth profiling revealed the presence of a heterogeneous layer, which was not observed in the STEM−EDX elemental mapping. This apparent discrepancy stems from the differences in the resolution of the STEM−EDX and XPS C_{60}^+ ion-beam sputtering techniques. Although both techniques probe the local chemical environment of the polyamide−polysulfone interfacial layer, the detection limit accuracy of these techniques is not comparable. For STEM, the relatively high electron beam voltage (i.e., 200 kV) resulted in a continuous background in the EDX signal, which precluded the detection of low concentration of elements with a high spatial resolution. The resulting spatial resolution for the STEM−EDX elemental mapping in the cross section image is not sufficient to detect the heterogeneous layer at the interfacial zone as the interfacial domain is mainly occupied by polysulfone. Conversely, the background contribution in XPS, mainly from inelastic scattering of electrons, can be subtracted without any loss of information. The background independent nature of the signal in our experiment, along with the intrinsic spatial resolution of the XPS signal (i.e., < 10 nm), allows the investigation of the interfacial domain of our system with the desired spatial resolution.

In summary, we demonstrate that both STEM−EDX and XPS C_{60}^+ ion-beam sputtering are powerful techniques for analyzing the nanostructure of the polyamide−polysulfone interface of TFC membranes. Further optimization of these interfacial characterization techniques will enable the elucidation of the mechanisms of interfacial polymerization, the gold-standard process for the fabrication of desalination membranes, and provide a better understanding of the relationship between membrane interfacial properties and performance. These techniques could also find applications in nanoscale characterization of other interfacial structures with similar elemental contrast.

■ ASSOCIATED CONTENT

Ⓢ Supporting Information

The Supporting Information is available free of charge on the ACS Publications website at DOI: 10.1021/acsami.5b05478.

Detailed descriptions of materials and methods as well as supporting figures and tables (PDF)

■ AUTHOR INFORMATION

Corresponding Authors

*E-mail: majun@hit.edu.cn. Tel: +86 451 86283010. Fax: +86 451 86283010

DOI: 10.1021/acsami.5b05478
ACS Appl. Mater. Interfaces 2015, 7, 16917−16922

*E-mail: menachem.elimelech@yale.edu. Phone: +1 203 432 2789. Fax: +1 203 432 4387

Author Contributions

†X.L. and S.N. contributed equally.

Notes

The authors declare no competing financial interest.

■ ACKNOWLEDGMENTS

Financial support from the Department of Defense through the Strategic Environmental Research and Development Program (SERDP, Project 12 ER01-054/ER-2217) and the Funds of the State Key Laboratory of Urban Water Resource and Environment (HIT, 2013DX05) is gratefully acknowledged. We also acknowledge the use of SEM and AFM facilities supported by the Yale Institute for Nanoscience and Quantum Engineering (YINQE) under NSF MRSEC DMR 1119826. This publication was developed under a graduate fellowship awarded by the China Scholarship Council to X.L.

■ REFERENCES

(1) Shannon, M. A.; Bohn, P. W.; Elimelech, M.; Georgiadis, J. G.; Marinas, B. J.; Mayes, A. M. Science and Technology for Water Purification in the Coming Decades. *Nature* **2008**, *452* (7185), 301−310.

(2) Elimelech, M.; Phillip, W. A. The Future of Seawater Desalination: Energy, Technology, and the Environment. *Science* **2011**, *333* (6043), 712−717.

(3) Petersen, R. J. Composite Reverse-Osmosis and Nanofiltration Membranes. *J. Membr. Sci.* **1993**, *83* (1), 81−150.

(4) Geise, G. M.; Lee, H. S.; Miller, D. J.; Freeman, B. D.; Mcgrath, J. E.; Paul, D. R. Water Purification by Membranes: The Role of Polymer Science. *J. Polym. Sci., Part B: Polym. Phys.* **2010**, *48* (15), 1685−1718.

(5) Kwak, S.-Y.; Yeom, M.-O.; Roh, I. J.; Kim, D. Y.; Kim, J.-J. Correlations of Chemical Structure, Atomic Force Microscopy (AFM) Morphology, and Reverse Osmosis (RO) Characteristics in Aromatic Polyester High-Flux RO Membranes. *J. Membr. Sci.* **1997**, *132* (2), 183−191.

(6) Vrijenhoek, E. M.; Hong, S.; Elimelech, M. Influence of Membrane Surface Properties on Initial Rate of Colloidal Fouling of Reverse Osmosis and Nanofiltration Membranes. *J. Membr. Sci.* **2001**, *188* (1), 115−128.

(7) Ghosh, A. K.; Jeong, B. H.; Huang, X. F.; Hoek, E. M. V. Impacts of Reaction and Curing Conditions on Polyamide Composite Reverse Osmosis Membrane Properties. *J. Membr. Sci.* **2008**, *311* (1−2), 34−45.

(8) Kwak, S.-Y.; Woo Ihm, D. Use of Atomic Force Microscopy and Solid-State Nmr Spectroscopy to Characterize Structure-Property-Performance Correlation in High-Flux Reverse Osmosis (RO) Membranes. *J. Membr. Sci.* **1999**, *158* (1), 143−153.

(9) Gu, J. E.; Lee, S.; Stafford, C. M.; Lee, J. S.; Choi, W.; Kim, B. Y.; Baek, K. Y.; Chan, E. P.; Chung, J. Y.; Bang, J.; Lee, J. H. Molecular Layer-by-Layer Assembled Thin-Film Composite Membranes for Water Desalination. *Adv. Mater.* **2013**, *25* (34), 4778−4782.

(10) Geise, G. M.; Park, H. B.; Sagle, A. C.; Freeman, B. D.; McGrath, J. E. Water Permeability and Water/Salt Selectivity Tradeoff in Polymers for Desalination. *J. Membr. Sci.* **2011**, *369* (1−2), 130−138.

(11) Freger, V. Nanoscale Heterogeneity of Polyamide Membranes Formed by Interfacial Polymerization. *Langmuir* **2003**, *19* (11), 4791−4797.

(12) Coronell, O.; Marinas, B. J.; Zhang, X. J.; Cahill, D. G. Quantification of Functional Groups and Modeling of Their Ionization Behavior in the Active Layer of FT30 Reverse Osmosis Membrane. *Environ. Sci. Technol.* **2008**, *42* (14), 5260−5266.

(13) Tang, C. Y. Y.; Kwon, Y. N.; Leckie, J. O. Probing the Nano- and Micro-Scales of Reverse Osmosis Membranes - a Comprehensive Characterization of Physiochemical Properties of Uncoated and Coated Membranes by XPS, TEM, ATR-FTIR, and Streaming Potential Measurements. *J. Membr. Sci.* **2007**, *287* (1), 146−156.

(14) Tiraferri, A.; Elimelech, M. Direct Quantification of Negatively Charged Functional Groups on Membrane Surfaces. *J. Membr. Sci.* **2012**, *389*, 499−508.

(15) Kim, S. H.; Kwak, S.-Y.; Suzuki, T. Positron Annihilation Spectroscopic Evidence to Demonstrate the Flux-Enhancement Mechanism in Morphology-Controlled Thin-Film-Composite (TFC) Membrane. *Environ. Sci. Technol.* **2005**, *39* (6), 1764−1770.

(16) Chan, E. P.; Young, A. P.; Lee, J. H.; Chung, J. Y.; Stafford, C. M. Swelling of Ultrathin Crosslinked Polyamide Water Desalination Membranes. *J. Polym. Sci., Part B: Polym. Phys.* **2013**, *51* (6), 385−391.

(17) Coronell, O.; Marinas, B. J.; Cahill, D. G. Depth Heterogeneity of Fully Aromatic Polyamide Active Layers in Reverse Osmosis and Nanofiltration Membranes. *Environ. Sci. Technol.* **2011**, *45* (10), 4513−4520.

(18) Song, Y.; Sun, P.; Henry, L. L.; Sun, B. Mechanisms of Structure and Performance Controlled Thin Film Composite Membrane Formation via Interfacial Polymerization Process. *J. Membr. Sci.* **2005**, *251* (1−2), 67−79.

(19) Prakash Rao, A.; Joshi, S. V.; Trivedi, J. J.; Devmurari, C. V.; Shah, V. J. Structure−Performance Correlation of Polyamide Thin Film Composite Membranes: Effect of Coating Conditions on Film Formation. *J. Membr. Sci.* **2003**, *211* (1), 13−24.

(20) Singh, P. S.; Joshi, S. V.; Trivedi, J. J.; Devmurari, C. V.; Rao, A. P.; Ghosh, P. K. Probing the Structural Variations of Thin Film Composite RO Membranes Obtained by Coating Polyamide over Polysulfone Membranes of Different Pore Dimensions. *J. Membr. Sci.* **2006**, *278* (1−2), 19−25.

(21) Kim, H. I.; Kim, S. S. Plasma Treatment of Polypropylene and Polysulfone Supports for Thin Film Composite Reverse Osmosis Membrane. *J. Membr. Sci.* **2006**, *286* (1−2), 193−201.

(22) Lu, X.; Arias Chavez, L. H.; Romero-Vargas Castrillón, S.; Ma, J.; Elimelech, M. Influence of Active Layer and Support Layer Surface Structures on Organic Fouling Propensity of Thin-Film Composite Forward Osmosis Membranes. *Environ. Sci. Technol.* **2015**, *49* (3), 1436−1444.

(23) Tiraferri, A.; Yip, N. Y.; Phillip, W. A.; Schiffman, J. D.; Elimelech, M. Relating Performance of Thin-Film Composite Forward Osmosis Membranes to Support Layer Formation and Structure. *J. Membr. Sci.* **2011**, *367* (1−2), 340−352.

(24) Ghosh, A. K.; Hoek, E. M. V. Impacts of Support Membrane Structure and Chemistry on Polyamide-Polysulfone Interfacial Composite Membranes. *J. Membr. Sci.* **2009**, *336* (1−2), 140−148.

(25) Kong, C. L.; Kanezashi, M.; Yamomoto, T.; Shintani, T.; Tsuru, T. Controlled Synthesis of High Performance Polyamide Membrane with Thin Dense Layer for Water Desalination. *J. Membr. Sci.* **2010**, *362* (1−2), 76−80.

(26) Freger, V. Swelling and Morphology of the Skin Layer of Polyamide Composite Membranes: An Atomic Force Microscopy Study. *Environ. Sci. Technol.* **2004**, *38* (11), 3168−3175.

(27) Pacheco, F. A.; Pinnau, I.; Reinhard, M.; Leckie, J. O. Characterization of Isolated Polyamide Thin Films of RO and NF Membranes Using Novel TEM Techniques. *J. Membr. Sci.* **2010**, *358* (1−2), 51−59.

(28) Yan, H.; Miao, X.; Xu, J.; Pan, G.; Zhang, Y.; Shi, Y.; Guo, M.; Liu, Y. The Porous Structure of the Fully-Aromatic Polyamide Film in Reverse Osmosis Membranes. *J. Membr. Sci.* **2015**, *475*, 504−510.

(29) Cui, Y.; Liu, X.-Y.; Chung, T.-S. Enhanced Osmotic Energy Generation from Salinity Gradients by Modifying Thin Film Composite Membranes. *Chem. Eng. J.* **2014**, *242*, 195−203.

(30) Jimenez Solomon, M. F.; Bhole, Y.; Livingston, A. G. High Flux Membranes for Organic Solvent Nanofiltration (OSN)—Interfacial Polymerization with Solvent Activation. *J. Membr. Sci.* **2012**, *423−424*, 371−382.

(31) Kurihara, M.; Hanakawa, M. Mega-ton Water System: Japanese National Research and Development Project on Seawater Desalination and Wastewater Reclamation. *Desalination* **2013**, *308*, 131−137.

DOI: 10.1021/acsami.5b05478
ACS Appl. Mater. Interfaces 2015, 7, 16917−16922

(32) Kamada, T.; Ohara, T.; Shintani, T.; Tsuru, T. Controlled Surface Morphology of Polyamide Membranes via the Addition of Co-Solvent for Improved Permeate Flux. *J. Membr. Sci.* **2014**, *467*, 303−312.
(33) Song, Y. Q.; Sheng, J.; Wei, M.; Yuan, X. B. Surface Modification of Polysulfone Membranes by Low-Temperature Plasma-Graft Poly-(Ethylene Glycol) onto Polysulfone Membranes. *J. Appl. Polym. Sci.* **2000**, *78* (5), 979−985.
(34) Hopkins, J.; Badyal, J. P. S. CF_4 Plasma Treatment of Asymmetric Polysulfone Membranes. *Langmuir* **1996**, *12* (15), 3666−3670.
(35) Klaysom, C.; Hermans, S.; Gahlaut, A.; Van Craenenbroeck, S.; Vankelecom, I. F. J. Polyamide/Polyacrylonitrile (PA/PAN) Thin Film Composite Osmosis Membranes: Film Optimization, Characterization and Performance Evaluation. *J. Membr. Sci.* **2013**, *445*, 25−33.

DOI: 10.1021/acsami.5b05478
ACS Appl. Mater. Interfaces 2015, 7, 16917−16922